Title: Adolescent Thalamocortical Inhibition Alters Prefrontal Excitation-Inhibition Balance

Abbreviated Title: Adolescent Thalamic Inhibition and Prefrontal Function

David Petersen[1,3], Ricardo Raudales[1,3], Ariadna Kim Silva[1,3], Christoph Kellendonk[1,2,3,#], Sarah Canetta[1,4,#],

[1]Department of Psychiatry, [2]Department of Molecular Pharmacology & Therapeutics, Vagelos College of Physicians and Surgeons, Columbia University Irving Medical Center, New York, NY 10032, USA

[3]Division of Molecular Therapeutics, [4]Division of Developmental Neuroscience, New York State Psychiatric Institute, New York, NY, 10032

[#]Equal contribution

*Correspondence: ck491@cumc.columbia.edu, ses2119@cumc.columbia.edu

33 Pages, 7 Figures, 119 words (abstract), 640 words (introduction), 1500 words (discussion)

Conflict of Interest Statement: The authors declare no competing financial interests.

Acknowledgments: This work was supported by NIMH R01MH128293 to C.K. and S.C and NIMH R01MH1282771 to S.C.

Abstract

Adolescent inhibition of thalamo-cortical projections from postnatal day P20-50 leads to long lasting deficits in prefrontal cortex function and cognition in the adult mouse. While this suggests a role of thalamic activity in prefrontal cortex maturation, it is unclear how inhibition of these projections affects prefrontal circuit connectivity during adolescence. Here, we used chemogenetic tools to inhibit thalamo-prefrontal projections in the mouse from P20-35 and measured synaptic inputs to prefrontal pyramidal neurons by layer (either II/III or V/VI) and projection target twenty-four hours later using slice physiology. We found a decrease in the frequency of excitatory and inhibitory currents in layer II/III nucleus accumbens (NAc) and layer V/VI medio-dorsal thalamus projecting neurons while layer V/VI NAc-projecting neurons showed an increase in the amplitude of excitatory and inhibitory currents. Regarding cortical projections, the frequency of inhibitory but not excitatory currents was enhanced in contralateral mPFC-projecting neurons. Notably, despite these complex changes in individual levels of excitation and inhibition, the overall balance between excitation and inhibition in each cell was only changed in the contralateral mPFC projections. This finding suggests homeostatic regulation occurs within subcortically but not intracortical callosally-projecting neurons. Increased inhibition of intra-prefrontal connectivity may therefore be particularly important for prefrontal cortex circuit maturation. Finally, we observed cognitive deficits in the adult mouse using this narrowed window of thalamocortical inhibition (P20-P35).

Significance Statement: Connectivity between two brain regions, the thalamus and the prefrontal cortex, has been found to be reduced in patients with schizophrenia. Neuronal activity in thalamo-cortical projections is important for the proper development of sensory cortices. How thalamo-cortical activity regulates prefrontal cortex development is less well understood. Here, we show that decreasing activity in thalamo-prefrontal projections in mice during early adolescence alters synaptic

connectivity to distinct neuronal projections within the prefrontal cortex that are already evident in adolescence. While some of these changes can be explained by reduced thalamo-cortical projections, other adaptations are intrinsic to the prefrontal cortex. These findings implicate adolescence as a critical period of cortical development and demonstrate this period as a potential target for therapeutic intervention.

Keywords

Adolescence, Excitation inhibition balance, Thalamocortical projections, Prefrontal cortex maturation

Introduction

The prefrontal cortex (PFC) supports high level cognitive functioning including working memory and other executive functions (Fuster, 2001; Miller et al., 2018). An impairment in the development or maturation of the prefrontal cortex during adolescence has been postulated to contribute to the cognitive deficits observed in patients with schizophrenia (Feinberg, 1982; Paus et al., 2008; Gogtay et al., 2011; Hoops and Flores, 2017; Larsen and Luna, 2018; Sakurai and Gamo, 2019; Chini and Hanganu-Opatz, 2021; Dienel et al., 2022; Yang and Tseng, 2022). Thalamic inputs regulate sensory cortical maturation during sensitive time windows of development (Wiesel and Hubel, 1963; Nabel and Morishita, 2013). We recently established in the mouse that thalamic input activity during adolescence is necessary for adult prefrontal cortex function and behavior (Benoit et al., 2022). More specifically, we found that decreasing activity in the mediodorsal thalamus from postnatal day 20-50 using pharmacogenetic tools led to deficits in the performance of two prefrontal dependent cognitive tasks addressing working memory and attentional set shifting. These deficits were measured in the adult mouse and associated with decreased anatomical thalamocortical projections and decreased functional excitatory post-synaptic currents measured in layer 2/3 prefrontal cortical pyramidal cells. Moreover, mice with thalamic inhibition during adolescence showed decreased correlated activity between neurons in the medial prefrontal cortex (mPFC) while performing an attentional set shifting task and the ability of the prefrontal cortex to decode task outcomes was impaired (Benoit et al., 2022). Notably, decreasing the activity of thalamo-prefrontal projections for a comparable length period in adulthood did not lead to the same long-lasting effects.

These findings established that thalamo-prefrontal activity is required during adolescence to sustain thalamocortical connectivity, prefrontal network function and cognitive behavior in adulthood. However, it was not clear whether these effects on circuit connectivity were apparent immediately after the

adolescent manipulation or if they require maturation into adulthood to manifest. Moreover, it was not clear whether the effects of decreased adolescent thalamo-prefrontal activity were restricted to the reduction of excitatory thalamic afferents or whether this manipulation led to more widespread changes in the intrinsic connectivity of the prefrontal cortex.

To address these questions, we undertook a detailed study of prefrontal cortical connectivity using slice electrophysiology twenty-four hours following pharmacogenetic inhibition of thalamo-prefrontal projections from postnatal day P20-35. We chose this reduced window of inhibition because prior work demonstrated changes in the density of thalamic projections to the mPFC following adolescent thalamic inhibition were already present at this time (Benoit et al., 2022). We first recorded excitatory and inhibitory currents from layer II/III neurons as previously done in the adult (Benoit et al., 2022) to establish whether the observed deficit in excitation arises during adolescence. We then restricted our recordings to specific mPFC projection neurons identified by their projection target and cortical layer. We found excitatory post synaptic currents are reduced in layer II/III cells during adolescence, as observed in adult mice. When analyzing specific projections, we found a reduction in frequency of excitatory and inhibitory currents to layer V/VI cortico-thalamic cells and layer II/III cortico-accumbens-projecting cells while layer V/VI cortico-accumbens-projecting neurons displayed increased amplitudes of excitatory and inhibitory currents. While we observed changes in excitation or inhibition in subcortically-projecting cells, the excitation/inhibition balance was not affected, suggesting homeostatic mechanisms may offset decreased excitatory inputs. In contrast, callosal cortico-cortical projection neurons displayed a significant decrease in E/I balance. Together, these data show a complex adaptation of cortical networks in response to decreased thalamo-cortical inputs during adolescence and suggest that activity in callosally-projecting cells in mPFC may be most profoundly affected due to a lack of homeostatic adaptation.

96 To determine whether this narrowed window (P20-P35) of adolescent thalamocortical inhibition would
97 impact cognitive flexibility in the adult mouse, we performed an attentional set shifting behavioral task.
98 Like P20-50 inhibition (Benoit et al., 2022) inhibition from P20-35 was sufficient to induced long lasting
99 deficits in cognition.
100

101 ## Materials and Methods

102 ### Animal Husbandry

103 All procedures were performed in accordance with guidelines approved by the Institutional Animal
104 Care and Use Committees at Columbia University and the New York State Psychiatric Institute
105 (protocol NYSPI 1589). Animals were housed under a 12-h light/12-h dark cycle in a temperature-
106 controlled environment (22 °C, humidity of 30–70%) with food and water available ad libitum, unless
107 otherwise noted. C57/ BL6 females and males (Jackson Laboratories, 000664) were used for all
108 experiments. Littermates were randomly assigned to each experimental group, with random
109 distribution across males and females. Mice were housed together with dams and littermates.
110 Offspring were weaned at P28, and group housed with same-sex littermates (no more than five mice
111 per cage). For thalamic inhibition, mice were given intraperitoneal (i.p.) injections of JHU37160
112 (J60, a CNO analog) dissolved in 0.9% sterile saline at 0.1 mg/kg twice per day (Bonaventura et al.,
113 2019). J60 was used as an alternative to the widely used clozapine-N-oxide (CNO) because J60 is
114 known to have less off-target effects. New evidence has shown CNO might be reverse metabolized
115 into clozapine, a common antipsychotic medication with high affinity to dopamine D2 and serotonin
116 2A receptors (Manvich et al., 2018). All mice were given J60 regardless of viral vector, except those
117 given saline with hM4D expression. Surgeries were conducted at P12-13, and all mice were injected
118 from P20 to P35. For electrophysiological experiments, 24 hours after the final J60 injection, mice

were anesthetized with isoflurane and decapitated for slice electrophysiology at P35 (+/- 4 days). For behavioral experiments, mice were tested in an attentional set shifting (ASST) task beginning in adulthood (>P90). Throughout data collection and analysis, experimenters were blinded to the group of the animal. We based sample sizes on previous experiments, and no statistical methods were used to calculate sample sizes.

Surgical Procedures

For viral injections at P13, mice were anesthetized with isoflurane and head-fixed in a stereotactic apparatus (Kopf). Mice were injected bilaterally in the midline thalamus with AAV5-hSyn-DIO-hM4D-mCherry (Addgene, 44362) or a control virus, AAV5-hSyn-DIO-mCherry (Addgene, 50459), at a volume of 0.25 µl (0.1µl/min). Mice were also injected bilaterally in the mPFC with retrograde AAV-hSyn-Cre-WPRE-hGH (Addgene, 105553) at a volume of 0.2 µl (0.1 µl/min). For the tracer experiments, mice were injected with retrograde AAV-hSyn-EGFP (Addgene, 50465) at a volume of 0.25 µl for the MD, 0.2 µl for the mPFC, and 0.1µl for the NAc. The following were the P13 coordinates: MD thalamus, −0.85 anterior–posterior (AP), ±0.20 medial–lateral (ML) and −3.25 dorsal–ventral (DV, zero at brain surface); mPFC, 2.4 AP, ±0.2 ML and −1.9 DV (zero at brain surface); NAc, 1.7 AP, ±1.1 ML and −5.07 DV. All coordinates were zeroed at bregma unless otherwise noted. Histology images were collected from each animal for each cohort, with at least 6 slices taken for each animal to determine viral spread and confirm targeting.

Slice Electrophysiology

140 Whole-cell voltage clamp recordings were performed in layer II/III mPFC pyramidal cells and layer
141 V/VI mPFC pyramidal cells. Recordings were obtained with a Multiclamp 700B amplifier
142 (Molecular Devices) and digitized using a Digidata 1440B acquisition system (Molecular Devices)
143 with Clampex 10 (Molecular Devices) and analyzed with pClamp 10 (Molecular Devices). Following
144 decapitation, 300-µm slices containing mPFC were incubated in artificial cerebral spinal fluid
145 containing 126mM NaCl, 2.5mM KCl, 2.0mM MgCl2, 1.25mM NaH2PO4, 2.0mM CaCl2, 26.2mM
146 NaHCO3 and 10.0mM d-glucose (pH 7.45, 310 mOsm) bubbled with oxygen at 32 °C for 30min
147 before being returned to room temperature for at least 1 hour before use. During recording, slices
148 were perfused in room temperature artificial cerebral spinal fluid at a rate of 5 ml/min. Electrodes
149 were pulled from 1.5-mm borosilicate glass pipettes on a P-97 puller (Sutter Instruments). Electrode
150 resistance was typically 1.5–3MΩ when filled with internal solution consisting of 130mM cesium
151 hydroxide monohydrate, 130mM D-gluconic acid, 10mM HEPES, 2.0mM MgCL2, 0.2mM EGTA,
152 2.5mM Mg-ATP, 0.3mM Na-GTP, and 5mM Lidocaine N-ethyl bromide (pH 7.3, 277mOsm).
153
154 *mPFC recordings.* Animals were sacrificed for recordings at P35 after the adolescent manipulation.
155 mPFC pyramidal cells were visually identified based on their shape and prominent apical dendrite at
156 ×40 magnification under infrared and diffusion interference contrast microscopy. Recordings were
157 taken from either layer II/III of the mPFC (PrL) or layer V/VI. Layer II/III was defined as any cell
158 lying 150µm-350µm from the pial surface. Layer V/VI was defined as cells within 400µm-600µm
159 from the pial surface. Spontaneous excitatory post synaptic currents (sEPSCs) were recorded in
160 voltage clamp at a holding potential of −65mV, and spontaneous inhibitory post-synaptic currents
161 (sIPSCs) were recorded in voltage clamp at a holding potential of +10mV. The combination of the
162 intracellular solution and the selected holding potentials allowed us to isolate EPSCs and IPSCs from

one another without the use of blockers, which we verified by demonstrating that sEPSCs were completed blocked by administration of 50 uM APV ((2R)-amino-5-phosphonovaleric acid) and 20 uM CNQX (6-cyano-7-nitroquinoxaline-2,3-dione), but not 20 uM bicuculine, and vice versa for sIPSCs.60 seconds of the current recording for each condition were analyzed. Recordings were filtered with a 2 kHz eight-pole low-pass Bessel filter, and sEPSCs and sIPSCs were detected using MiniAnalysis (Synaptosoft). Frequency, amplitude, and instantaneous frequency were calculated for all traces. Frequency was calculated by dividing the total number of events by time (60s). Amplitude was the distance from baseline to the tip of the event. Instantaneous frequency was the inverse of the interevent-interval converted to a frequency. All event data were averaged by cell.

Attentional Set Shifting Behavioral Task

At P90, mice were gradually restricted to 85% of their body weight. Mice were habituated to the testing arena on day 1. On days 2–3, they were trained to dig in both bedding media (corn cob and paper pellet, both unscented) to obtain a food reward. Once mice dug reliably, testing began. For each trial, mice were placed at the opposite end from two terra cotta bowls containing different odor/medium combinations. For IA, mice needed to learn that the cinnamon scent, not the paprika scent, predicted a Honey Nut Cheerio reward, irrespective of the bedding medium. For the first five trials, mice could explore both bowls until they found the reward, but the trial was only scored as correct if the animal initially chose the correct bowl. From the sixth trial onward, once the mouse began digging in a bowl, the entrance to the other bowl was closed off. The criterion was reached when the mouse made eight of ten consecutive correct choices. If the mouse did not meet the criterion in 30 trials, the animal did not advance to the next stage. If the mouse did reach the criterion, the extra-dimensional set shifting (EDSS) portion of the task began. In EDSS, the animal needed to learn that the type of bedding medium (paper pellets, not corn cobs) predicted

186 the Honey Nut Cheerio reward irrespective of odor. The criterion was reached when the mouse made eight
187 of ten consecutive correct choices. All behavioral tasks were conducted during the light cycle.
188

189 **Statistics**

190 Statistical analysis and graph preparations were done using Prism 9 software (GraphPad Software),
191 JASP (JASP Team (2023), JASP (Version 0.17.3)) or custom scripts in R. Linear mixed effects
192 models with individual animal used as a random-effects grouping factor were used to analyze slice
193 physiology. Linear mixed effects models were used over a common ANOVA or t-test to account for
194 the possible non-independence of measurements from cells from the same animal. Prior to analysis,
195 all datasets were tested for outliers, and they were removed using the following equation (Q1-1.5 x
196 IQR or Q3 + 1.5 x IQR), which identifies datapoints +/- 2.698σ from the mean. For the nonspecific
197 L II/III experiment, 2 outliers were removed from the EPSC hM4D+Saline amplitude group, 1 outlier
198 was removed from the IPSC hM4D frequency group, and 1 outlier was removed from the IPSC hM4D
199 instantaneous frequency group. For the cortico-accumbens experiment, 2 outliers were removed from
200 the IPSC hM4D group. For the cortico-cortical population experiment, 2 outliers were removed from
201 the IPSC mCherry frequency group. For the E/I balance analysis, 2 outliers were removed from the
202 hM4D cortico-cortical frequency group. An independent samples t-test was used to analyze behavior.

203 **Results**

204 **Adolescent thalamocortical activity regulates excitatory transmission to superficial**
205 **mPFC.**

206 We first performed patch clamp recordings in brain slices from prelimbic layer II/III neurons, which is the
207 mPFC population of projection neurons that obtain the most prominent input from the MD (Anastasiades
208 and Carter, 2021). To inhibit thalamic activity during adolescence on postnatal day 13 (P13), we injected
209 an adeno-associated virus (AAV) carrying a Cre-dependent version of the inhibitory designer receptor
210 hM4D into the thalamus of C57 mice and a retrograde virus carrying Cre recombinase, rgAAV-CRE, into
211 the mPFC. Retrograde transport will cause Cre recombinase expression in the MD, leading to hM4D
212 expression selectively in medial prefrontal-projecting neurons (Fig. 1a). We then chronically inhibited
213 these cortically-projecting MD cells with the hM4D ligand JHU37160 (J60) (0.1 mg/kg) from postnatal
214 day 20 until the day before they were recorded (P35±4days) (Fig. 1b). To control for the possible non-
215 ligand-dependent effects of the hM4D receptor, we also included a group of mice expressing hM4D that
216 were injected with saline during the same developmental window. Twenty-four hours after the last J60
217 injection (at P35±4days), we recorded layer II/III neurons and analyzed excitatory and inhibitory post-
218 synaptic currents.

219

220 Using linear mixed effects models, we found that inhibition of thalamo-cortical projections from P20-35
221 decreased the frequency [$F(2, 5.93) = 6.854$, $p = 0.029$] and spatial distribution (instantaneous frequency)
222 [$F(1,7.02) = 8.129$, $p = 0.025$] of spontaneous excitatory currents (sEPSCs), while there was no change in
223 the amplitude [$F(2, 42) = 1.763$, $p = 0.184$] of sEPSCs when compared to controls (Fig. 1f-i). Measuring
224 spontaneous inhibitory currents (sIPSCs) resulted in a trend of diminished frequency [$F(2, 9.78) = 2.906$,
225 $p = 0.102$] while spatial distribution (instantaneous frequency) [$F(2, 10.92) = 1.973$, $p = 0.185$] and

226 amplitude [$F(2, 8.41) = 0.458$, $p = 0.458$] remained unchanged when compared to controls (Fig. 1f-i).
227 Furthermore, when comparing the mCherry and Saline groups in a post-hoc contrast, no significant
228 differences were observed, signaling the lack of non-ligand dependent effects of the hM4D receptor (EPSC
229 frequency [$z(\infty) = 0.501$, $p_{bonferroni} = 1.000$]; EPSC median instantaneous frequency [$z(\infty) = 1.097$,
230 $p_{bonferroni} = 0.818$]; and no overall effect in EPSC amplitude, IPSC frequency, IPSC instantaneous
231 frequency, or IPSC amplitude. These results indicate that adolescent thalamocortical activity causes
232 significant alterations to excitatory transmission in the superficial regions of the mPFC, consistent with
233 what we previously found in adult mice. (Benoit et al., 2022).
234

235 **Adolescent thalamocortical activity regulates excitatory and inhibitory transmission to**
236 **superficial layer II/III cortico-accumbens projections.**

237 We then determined whether the observed effects of adolescent thalamocortical inhibition includes the
238 layer II/III cortico-accumbens cell populations. To this end, we injected the rgGFP virus into the nucleus
239 accumbens (NAc) (Fig. 2a-b) and recorded from the superficial layers (II/III) of the mPFC. We found that
240 in superficial NAc-projecting neurons, excitatory and inhibitory transmission were both dampened
241 following adolescent thalamo-cortical inhibition. For excitatory currents, the frequency [$F(1, 47) = 9.354$,
242 $p = 0.004$] was significantly decreased but not the spatial distribution (instantaneous frequency) [$F(1,$
243 $6.77) = 1.926$, $p = 0.208$] or the amplitude [$F(1, 6.19) = 3.313$, $p = 0.117$] (Fig. 2e-f). For inhibitory
244 transmission in superficial layers, sIPSC frequency was reduced [$F(1, 4.89) = 9.451$, $p = 0.028$] but not the
245 spatial distribution (instantaneous frequency) [$F(1, 7.79) = 0.955$, $p = 0.358$] or the amplitude [$F(1, 7.03)$
246 $= 3.402$, $p = 0.107$] (Fig. 2g-h). These data show that excitatory and inhibitory inputs are decreased onto
247 layer II/III accumbens-projecting neurons.
248

249 **Adolescent thalamocortical activity regulates excitatory and inhibitory transmission to**
250 **cortico-thalamic projections.**

251 We then determined the effects of chronic thalamocortical inhibition on a different subcortical projection,
252 cortical cells from deep layers V/VI projecting to the MD thalamus. A rgGFP virus was injected into the
253 MD and whole cell patch clamp recordings were taken in thalamic-projecting cortical cells (Fig. 3a-b).
254 Like for non-specific layer II/III and cortico-accumbens neurons, we observed significant decreases in
255 excitatory synaptic transmission (Fig. 3e-h). Significant decreases were observed in both the frequency
256 [$F(1, 6.73) = 12.960$, $p = 0.009$] and spatial distribution (instantaneous frequency) [$F(1, 6.10) = 13.045$,
257 $p = 0.011$] of sEPSCs but the amplitude [$F(1, 5.36) = 0.689$, $p = 0.442$] of sEPSCs remained unchanged
258 (Fig. 3e-f). In addition, the frequency [$F(1, 6.39) = 7.829$, $p = 0.029$] and spatial distribution (instantaneous
259 frequency) [$F(1, 5.96) = 6.501$, $p = 0.044$] but not the amplitude [$F(1, 4.77) = 0.991$, $p = 0.367$] of sIPSCs
260 was reduced after P20-35 thalamic inhibition (Fig. 3g-h). These data show that, like for superficial layer
261 II/III accumbens projections, adolescent thalamo-prefrontal inhibition also decreases excitatory and
262 inhibitory synaptic inputs to deep layer cortico-thalamic neurons.
263

264 **Adolescent thalamocortical activity regulates the amplitude of excitatory and**
265 **inhibitory currents in deep layer (V/VI) accumbens-projecting cortical cells.**

266 Accumbens-projecting prefrontal neurons are located in both superficial and deep cortical layers
267 (Anastasiades and Carter, 2021). We therefore also recorded accumbens-projecting cells in layer V/VI.
268 We found significant increases to excitatory and inhibitory current amplitude, and no changes in frequency
269 or spatial distribution, in deep layer accumbens-projecting cells (Fig 4e-h). When measuring excitatory
270 currents in deep layers, amplitude was significantly increased [$F(1, 29) = 8.976$, $p = 0.006$] however,
271 frequency [$F(1, 5.49) = 7.841\text{x}10^{-5}$, $p = 0.993$] and spatial distribution (instantaneous frequency) [$F(1,$

272 6.24) = 0.196, p =0.673] remained unchanged (Fig 4e-f). Similar to excitatory transmission, for inhibitory
273 currents in deeper layers, amplitude was significantly increased [F(1, 4.25) = 14.809, p =0.013] however,
274 frequency [F(1, 6.82) = 0.417, p =0.539] and spatial distribution (instantaneous frequency) [F(1, 6.53) =
275 0.910, p =0.374] remained unchanged (Fig. 4 g-h). Thus, unlike layer II/III accumbens projection neurons,
276 excitatory and inhibitory drive onto layer V/VI accumbens neurons is not decreased but it is enhanced
277 although at the level of amplitude and not frequency.
278

279 **Adolescent thalamocortical activity regulates cross-hemispheric inhibition.**

280 To determine how adolescent thalamocortical inhibition impacts cortico-cortical circuitry, a rgGFP virus
281 was injected into the dextral prelimbic mPFC and whole cell patch clamp recordings were taken in
282 callosally-projecting cortical cells in the sinistral hemisphere (Fig. 5a-b). No significant differences were
283 observed in the frequency [F(1, 7.41) = 0.012, p = 0.917], spatial distribution (instantaneous frequency)
284 [F(1, 7.30) = 0.399, p = 0.547] or amplitude) [F(1, 6.37) = 2.865, p = 0.134] of excitatory events in
285 cortical-projecting cortical cells (Fig. 5e-f). Unlike excitatory transmission, inhibitory transmission
286 significantly increased in the distribution of events (instantaneous frequency) [F(1, 5.95) = 8.023, p =
287 0.030] and trended in frequency [F(1, 7.32) = 4.185, p = 0.078] but not amplitude [F(1, 62) = 0.112, p
288 = 0.912] after adolescent thalamocortical inhibition (Fig. 5g-h). These findings were unexpected since
289 callosally-projecting prelimbic neurons are enriched in layer II/III (Anastasiades et al., 2018) and the non-
290 selective analysis of layer II/III neurons displayed a decrease in the frequency of excitatory currents and
291 no increase in inhibition.
292

293 **Excitation-Inhibition balance is only altered in callosally-projecting mPFC neurons.**

294 Excitation and inhibition are well calibrated in cortical neurons (Okun and Lampl, 2008) and in agreement
295 with this we found a strong correlation in the frequency of excitatory and inhibitory currents for non-
296 specific layer II/III cortical cells [R^2=0.524, P<0.001], cortico-accumbens cells [R^2=0.811, P<0.001],
297 cortico-thalamic [R^2=0.850, P<0.001], and cortico-cortical cells [R^2=0.550, P<0.001]. In many cell
298 populations, we observed changes in both excitation and inhibition, suggesting homeostatic mechanisms
299 may compensate for reduced excitatory drive from the thalamus. We therefore calculated the excitation
300 inhibition-balance in the different analyzed population of neurons. No changes in the excitation-inhibition
301 balance were measured in layer II/III and V/VI cortico-accumbens-projecting neurons, and cortico-
302 thalamic neurons (Fig. 6b-e). In contrast, when analyzing the ratio of excitatory to inhibitory currents in
303 contralaterally-projecting mPFC neurons, the frequency [$F(1, 11.37) = 5.697$, $p = 0.035$] and spatial
304 distribution (instantaneous frequency) [$F(1, 9.34) = 5.744$, $p = 0.039$] of excitatory to inhibitory currents
305 was significantly weighted towards inhibition (Fig. 6f).
306
307 **P20-P35 thalamocortical inhibition produces cognitive deficits in adult mice.**
308 We then determined whether thalamocortical inhibition from P20-P35 has similar long-lasting effects on
309 cognition compared to P20-50 inhibition. J60 was administered from P20-P35 to mice expressing hM4D
310 or a control fluorophore (GFP) in thalamus-prelimbic cortex-projecting neurons. Behavioral testing was
311 conducted 55 days later, at P90 (Fig. 7a). After thalamocortical inhibition, at P90, mice performed the
312 attentional set-shifting task (ASST). For initial acquisition, mice were trained to associate a cinnamon
313 scent with a reward irrespective of bedding medium. After meeting criterion, an extra-dimensional set
314 shift (EDSS) occurred, and mice had to associate the paper bedding with a reward irrespective of scent
315 (Fig. 7d). Adolescent thalamo-prefrontal inhibition did not affect the initial acquisition of the task
316 [t=0.9647, df=22, p=0.3452] but delayed acquisition of the extra-dimensional set shift compared to

317 controls [t=2.442, df=22, *p=0.0354] (Figure 7e). Adolescent-inhibited hM4D animals committed more
318 perseverative errors than control animals [t=2.461, df=22, *p=0.0222] (Figure 7f). Perseverative errors
319 are when the mouse continues with the same response strategy following a set shift. However, adolescent-
320 inhibited hM4D animals also committed more random errors than control animals and the deficit was not
321 due to a specific error type [t=2.786, df=22, *p=0.0108] (Figure 7f). These data indicate that a restricted
322 critical window (P20-P35) is sufficient to manifest deficits observed with a longer period of inhibition
323 (P20-P50) (Benoit et al., 2022).
324

325 **Discussion**

326 To determine thalamocortical activity's importance for prefrontal circuit maturation we inhibited thalamo-
327 mPFC projections from P20-35 and recorded from prelimbic neurons twenty-four hours later. We made
328 several observations. First, our findings reveal that excitatory transmission to layer-II/III is already
329 decreased during adolescence, suggesting the adult excitation loss (Benoit et al., 2022) does not require
330 maturation to adulthood but arises during adolescence. Second, we measured decreased excitatory and
331 inhibitory transmission to layer-II/III NAc- and layer-V/VI thalamic-projecting neurons. These inhibitory
332 changes suggest adolescent-thalamocortical-inhibition leads to alterations in prefrontal connectivity
333 beyond the loss of excitatory thalamic input, previously observed at the anatomical level at P35 (Benoit
334 et al., 2022). Third, we observed a surprising increase in excitatory and inhibitory transmission to layer-
335 V/VI NAc-projecting neurons in amplitude but not frequency, suggesting a post-synaptic adaptation.
336 While the specificity of this effect is unclear, NAc-projecting cells in deep layers have distinct molecular
337 characteristics from superficial layers, which may differentially impact their response to adolescent-
338 thalamocortical-inhibition (Bhattacherjee et al., 2019). Fourth, we measured enhanced inhibition in
339 cortico-cortical connectivity, providing further evidence for a complex adaptation in response to

340 adolescent-thalamocortical-inhibition. Intriguingly, while excitatory and inhibitory (E/I) drive was
341 altered onto subcortical projection neurons, a change in the E/I balance was only measured in cross-
342 hemispheric mPFC projections and not in the three subcortical projections analyzed. As functional
343 stability in neural circuits can be sustained by homeostatic re-balancing of E/I inputs, the largest functional
344 effect of adolescent-thalamocortical-inhibition on prefrontal circuitry may be a decrease in the activity
345 of callosally-projecting mPFC pyramidal cells. While difficult to predict neuronal activity in-vivo from
346 slice physiology, enhanced inhibition, and less activation of callosal-projecting neurons during
347 adolescence might have long-lasting consequences for mPFC function. Finally, we established that this
348 narrowed window of inhibition (P20-P35) is sufficient to produce cognitive deficits in the adult mouse.
349

350 **Decreased excitatory and inhibitory transmission in mPFC arises during adolescence.**

351 Previous work demonstrated that adolescent-thalamocortical-inhibition (P20-P50) resulted in
352 cognitive and physiological deficits in the adult mouse, including a loss of excitatory transmission
353 in non-projection-specific layer-II/III pyramidal cells. Here, we observe deficits are established
354 during adolescence, prior to being sustained into adulthood. This excitatory dampening onto layer-
355 II/III neurons could result from the loss of MD innervation to pyramidal cells and/or a loss of local
356 excitation. The bimodal distribution of the effects in layer-II/III led us to hypothesize that adolescent
357 thalamocortical-inhibition may be differentially affecting subpopulations of neurons in the
358 subregion.
359 Excitatory and inhibitory currents were both decreased in NAc-projecting pyramidal cells following
360 adolescent-thalamocortical-inhibition. These data show that adolescent-thalamocortical-inhibition
361 may have widespread effects on diverse cell populations, including mPFC-NAc projections that are

362 essential for reward driven motivated behaviors (Kalivas et al., 2005; Mannella et al., 2013;
363 McGlinchey et al., 2016).
364 The decrease in inhibitory transmission could be due to a reduction in thalamic projections onto
365 interneurons (Yang et al., 2021). The MD directly innervates layer-II/III parvalbumin (PV+) and other
366 interneurons, providing a source of feedforward inhibition to cortical projection neurons (Delevich et al.,
367 2015; Canetta et al., 2020). Changes in interneuron-driven inhibition in NAc-projecting cells measured in
368 slice could reflect either reduced excitatory drive onto PV+ cells, or adaptations within PV+ interneurons
369 following thalamic inhibition. To determine whether adolescent-thalamocortical-inhibition also alters
370 excitatory and inhibitory connections in deeper layers of the mPFC, we next recorded from cortico-
371 thalamic neurons in layer-V/VI.
372 We found that adolescent thalamocortical-inhibition resulted in a decrease in the frequency of
373 excitatory and inhibitory currents in thalamus-projecting cells in layer-V/VI of the mPFC, like the
374 effects seen in superficial NAc-projecting cells. The MD primarily projects to layer-II/III; however,
375 slice physiology has demonstrated monosynaptic, direct-reciprocal connection to the deeper layers
376 (V/VI) of the cortex (Collins et al., 2018). The origins for the excitatory and inhibitory decrease may
377 therefore be like the ones measured in layer-II/III.
378

379 **Deeper accumbens-projecting cells show post-synaptic adaptations to MD inhibition.**

380 Surprisingly, we found that following adolescent-thalamocortical-inhibition, the amplitude of
381 excitatory and inhibitory currents increased in layer-V/VI accumbens-projecting neurons**,** while the
382 frequency and spatial distribution remained the same. Changes in amplitude are thought to reflect
383 post-synaptic alterations, this amplitude increase may therefore be a post-synaptic adaptation. It is
384 unclear; however, for what the increased amplitude would be compensating. Although the thalamus

makes direct connections onto deep layer pyramidal cells (Collins et al., 2018), it is unknown whether the MD directly innervates deep NAc-projecting cells.

Adolescent-thalamocortical-inhibition increases inhibitory inputs to callosally-projecting neurons.

The frequency of excitatory inputs to callosally-projecting mPFC neurons did not change following adolescent-thalamocortical-inhibition; however, inhibitory inputs were increased. The absence of excitatory transmission changes in this population is surprising, given they receive strong MD inputs (Anastasiades et al., 2018). Why excitatory inputs to this population are spared remains unknown, but it suggests that excitatory inputs from other brain regions may offset the reduction in excitatory inputs from the thalamus. The increase in inhibitory transmission is also surprising given that inhibition was decreased in NAc-projecting cells found in the same cortical layer. Moreover, while changes in E/I, driven by adolescent-thalamocortical-inhibition largely scaled in all other populations, cortico-cortical-projecting cells showed a significant reduction in their sE/IPSC ratio. Overall, E/I ratio stability following adolescent thalamocortical-inhibition displays homeostatic regulation in subcortically projecting neurons as inhibition may be an adaptive consequence to the decrease in excitatory thalamic inputs. However, in cortically projecting neurons, adolescent thalamocortical-inhibition resulted in an inhibitory increase with no effect on excitation, and a significant reduction in E/I balance in these cells. Thus, callosally-projecting neurons may not undergo homeostatic adaptation compared to subcortically-projecting cells. Work in the somatosensory cortex shows subcortically-projecting neurons in layer-V display faster synaptic depression and homeostatic rebound compared to cortically-projecting layer-V cells (Greenhill et al., 2015). If conserved in layer-II/III of the mPFC, this could be a rationale for delayed homeostatic

408 adaptation in cortically-projecting cortical cells. Therefore, we predict cortically-projecting neurons
409 might experience the greatest change following adolescent-thalamocortical-inhibition, with the net
410 effect of being less active in vivo. This change may in turn contribute to a loss of cross-hemispheric
411 cortical communication, hypothesized to be important for cognitive processes (Hasegawa et al.,
412 1998; Holler-Wallscheid et al., 2017). These effects may depress cortical output to other neural
413 circuits, having widespread effects on prefrontal network function.
414 Alternatively, the increase in callosal inhibition following adolescent-thalamocortical-inhibition may
415 have resulted from interneuron-mediated disinhibition via somatostatin (SST+), vasoactive intestinal
416 polypeptide (VIP+), and PV+ interneurons. Both VIP+ and SST+ interneurons receive MD input and
417 inhibit other interneurons including PV+ interneurons (Ahrlund-Richter et al., 2019; Sun et al., 2019;
418 Canetta et al., 2020). Therefore, the overall increase in inhibition could be due to complex disinhibition
419 between VIP+, SOM+, PV+ and pyramidal cell types. It is unclear why it should be specific only to
420 callosal, intracortical connectivity but some interneurons target callosal projecting pyramidal cells (Pi et
421 al., 2013; Cho et al., 2023).
422
423 **Possible mechanisms of mPFC plasticity induced by adolescent-thalamocortical-inhibition.**
424 Recent studies also point to intra-cortical mechanisms mediating maturation of cortical circuitry. Anterior
425 cingulate (ACC) neurons show greater excitatory synaptic inputs during adolescence than adulthood and
426 inhibition of ACC to visual cortex projection neurons during adolescence disrupts the maintenance of local
427 connectivity within the ACC (Nabel et al., 2020). By analogy, if adolescent-thalamocortical-inhibition
428 decreases activity of mPFC-thalamic or accumbens projection neurons during adolescence, this may lead
429 to a disruption in the maintenance of local excitation in the mPFC. A different mechanism has been
430 described within the visual cortex. Here, inhibition of layer-II/III neurons during the critical period of

431 primary visual cortex development (P24-29) led to excitatory synaptic scaling and increased intrinsic
432 excitability suggesting homeostatic plasticity as a mechanism affecting visual cortex maturation (Wen and
433 Turrigiano, 2021). Further studies on synaptic scaling could identify the plasticity mechanisms in mPFC
434 circuitry induced by adolescent-thalamocortical-inhibition.
435
436 **A narrowed window of adolescent-thalamocortical-inhibition regulates adult cognition.**
437 Adolescent-thalamocortical-inhibition from P20-35 elicited similar deficits in attentional set shifting the
438 adult mouse at P90 window compared to a broader time window from P20-50 (Benoit et al., 2022). This
439 narrows the sensitive window, implicating early adolescence as a critical period during which thalamic
440 input regulates prefrontal cortex development.
441
442 **Conclusions:**
443 In sum, our data demonstrate adolescent-thalamocortical-inhibition results in projection specific
444 changes in synaptic connectivity in the mPFC that become evident already during adolescence. The
445 dysregulation of multiple neural circuits demonstrates a widespread effect of adolescent-thalamocortical-
446 inhibition that impacts more than just thalamocortical circuitry and deficits cannot be explained solely by
447 a lack of anatomical input. Rather, they generate widespread adaptative and possibly maladaptive
448 physiological responses within prefrontal circuitry.
449
450 **Future Directions:**
451 Future studies directly measuring excitatory and inhibitory currents and using optogenetic approaches to
452 probe functional connectivity in interneurons and pyramidal cells will be able to address how these
453 complex adaptations arise. Studies exploring how these physiological changes will scale into adulthood

454 will be of interest. If they do, it is likely adolescent-thalamocortical-inhibition would lead to changes in
455 prefrontal circuitry that are 'hardwired' into adulthood. Alternatively, changes identified in adolescence
456 may be transient, setting in motion altered adult prefrontal function. Finally, future research will address
457 whether disinhibition of callosal-cortical-projecting cells during adolescence following adolescent-
458 thalamocortical-inhibition will rescue long-term negative effects and determine whether adolescence is
459 a potential target for therapeutic intervention.

460 **Figure Legends:**

461 **Figure 1) Adolescent thalamocortical activity regulates excitatory transmission to superficial**
462 **mPFC**. **a**, Adolescent experimental timeline, and schematic. Whole-cell patch clamp recordings were
463 made from pyramidal cells in layer II/III of the mPFC from hM4D and control mice. These pyramidal
464 cells receive excitatory inputs from the thalamus as well as inhibitory inputs from local interneurons;
465 created with https://biorender.com. **b**, Example image illustrating hM4D-mCherry expression in the
466 mediodorsal thalamus (dotted outline) in adolescent animals. Scale bar represents 300µm. **c**, Example
467 image illustrating the recording location in the prelimbic (PrL) subregion (orange dotted outline) of
468 the medial prefrontal cortex. All recordings for this experiment were conducted in this region
469 approximately 200-350µm from the pial surface (L II/III) denoted by the orange dotted line.
470 Recording pipette outlined in white. Scale bar represents 500µm **d**, Representative traces showing
471 sEPSCs of hM4D animals and mCherry controls. **e**, Representative traces showing sIPSCs of hM4D
472 animals and mCherry controls. **f**, sEPSC frequency (right) and median instantaneous frequency
473 (middle) is significantly reduced following adolescent thalamic inhibition relative to control mice,
474 but sEPSC amplitude (left) is unchanged; mCherry control, $n = 26$ cells and 6 animals; hM4D, $n = 14$
475 cells and 5 animals; hM4D+Saline n=9 cells and 2 animals; frequency: mCherry control
476 4.617(3.050) Hz, hM4D 2.833(3.858) Hz, and hM4D+Saline 5.733(2.700) Hz, contrasts of estimated
477 marginal means revealed a significant difference between hM4D animals and both mCherry, $z = -$
478 $3.311.129$, d.f. = ∞ $*P_{bonferroni} = 0.003$, and hM4D+Saline, $z = 3.035$, d.f. = ∞ $*P_{bonferroni} = 0.007$ but
479 no significant difference between mCherry and hM4D+Saline, $z = 0.501$, d.f. = ∞ $*P_{bonferroni} = 1.000$;
480 median instantaneous frequency: mCherry control 7.892(5.340) Hz, hM4D 5.126(4.882) Hz,
481 hM4D+Saline 10.005(4.989) Hz; contrasts of estimated marginal means revealed a significant
482 difference between hM4D animals and both mCherry, $z = -3.032$, d.f. = ∞ $*P_{bonferroni} = 0.007$, and

483 hM4D+Saline, $z = 3.348$, d.f. = ∞ *$P_{bonferroni} = 0.002$ but no significant difference between mCherry
484 and hM4D+Saline, $z = 1.097$, d.f. = ∞ *$P_{bonferroni} = 0.818$; amplitude: mCherry control
485 18.785(5.250) pA, hM4D 20.916(4.882) pA, and hM4D+Saline 28.786(5.782) pA. All reported
486 values are Median(Interquartile Range). **g**, Graph of the cumulative firing distribution for sEPSCs in
487 L 2/3 pyramidal cells in the mPFC, IEI represents the interevent-interval between spontaneous
488 events. **h**, sIPSC frequency (right) may trend downwards but median instantaneous frequency
489 (middle) and amplitude (left) are unchanged following adolescent thalamic inhibition relative to
490 control mice; mCherry control, $n = 26$ cells and 6 animals; hM4D, $n = 14$ cells and 5 animals;
491 frequency: mCherry control 2.500(3.267) Hz, hM4D 1.000(0.550) Hz and hM4D+Saline
492 2.717(1.833); median instantaneous frequency: mCherry control 3.826(5.039) Hz, hM4D
493 1.989(1.256) Hz, and hM4D+Saline 4.014(2.366; amplitude: mCherry control 14.264(5.638) pA,
494 hM4D 14.3(6.075) pA, and hM4D+Saline 18.849(6.737). All reported values are
495 Median(Interquartile Range). **i**, Graph of the cumulative firing distribution for sIPSCs in L 2/3
496 pyramidal cells in the mPFC, *P<0.05, #P~0.10.
497
498 **Figure 2) Adolescent thalamocortical activity regulates excitatory and inhibitory transmission**
499 **to superficial layer II/III cortico-accumbens projections. a**, Adolescent experimental timeline and
500 schematic. Whole-cell patch clamp recordings were made from accumbens-projecting pyramidal
501 cells in layer II/III of the mPFC from hM4D and control mice; Created with https://biorender.com. **b**,
502 Example image illustrating rgGFP positive, accumbens-projecting cells in the prelimbic subregion
503 of the medial prefrontal cortex, orange dotted outline represents layer II/III. Scale bar represents
504 500µm. **c**, Representative traces showing sEPSCs of hM4D animals and mCherry controls. **d**,
505 Representative traces showing sIPSCs of hM4D animals and mCherry controls**. e**, sEPSC frequency

506 (right) is significantly reduced in accumbens-projecting cortical cells following adolescent thalamic
507 inhibition relative to control mice, but sEPSC amplitude (left) and median instantaneous frequency
508 (middle) are unchanged; mCherry control, $n = 21$ cells and 5 animals; hM4D, $n = 28$ cells and 6
509 animals; frequency: mCherry control 5.367(2.717) Hz, hM4D 2.975(1.871) Hz.; median
510 instantaneous frequency: mCherry control 8.514(4.842) Hz and hM4D 5.579(4.803) Hz; amplitude:
511 mCherry control 21.051(7.992) pA and hM4D 23.648(12.495) pA. All reported values are
512 Median(Interquartile Range). **f**, Graph of the cumulative firing distribution for sEPSCs in L II/III
513 accumbens-projecting pyramidal cells in the mPFC, IEI represents the interevent-interval between
514 spontaneous events. **g**, sIPSC frequency (right) is significantly reduced in accumbens-projecting
515 cortical cells following adolescent thalamic inhibition relative to control mice, but sIPSC amplitude
516 (left) and median instantaneous frequency (middle) are unchanged; mCherry control, $n = 21$ cells and
517 5 animals; hM4D, $n = 28$ cells and 6 animals; frequency: mCherry control 3.350(2.350) Hz, hM4D
518 1.417(1.762) Hz; median instantaneous frequency: mCherry control 5.195(4.817) Hz and hM4D
519 2.776(2.753) Hz; amplitude: mCherry control 14.618(3.768) pA and hM4D 17.597(7.919) pA. All
520 reported values are Median(Interquartile Range). **h**, Graph of the cumulative firing distribution for
521 sIPSCs in L II/III accumbens-projecting pyramidal cells in the mPFC. *P<0.05.
522
523
524 **Figure 3) Adolescent thalamocortical activity regulates excitatory and inhibitory transmission**
525 **to cortico-thalamic projections. a**, Adolescent experimental timeline, and schematic. Whole-cell
526 patch clamp recordings were made from cortical-projecting pyramidal cells in layer V/VI of the
527 mPFC from hM4D and control mice. These pyramidal cells receive excitatory inputs from the
528 thalamus and superficial layers of the cortex as well as inhibitory inputs from local interneurons;

529 created with https://biorender.com. **b**, Example image illustrating rgGFP positive cells in the
530 prelimbic subregion of the medial prefrontal cortex. All recordings for this experiment were
531 conducted in this region approximately 500-600µm from the pial surface L V/VI (yellow outline).
532 Scale bar represents 300µm **c**, Representative traces showing sEPSCs of hM4D animals and mCherry
533 controls. **d**, Representative traces showing sIPSCs of hM4D animals and mCherry controls**.** **e**, sEPSC
534 frequency (right) and median instantaneous frequency (middle) is significantly reduced in thalamic-
535 projecting cortical cells following adolescent thalamic inhibition relative to control mice, but sEPSC
536 amplitude (left) is unchanged; mCherry control, $n = 19$ cells and 4 animals; hM4D, $n = 26$ cells and
537 5 animals; frequency: mCherry control 6.717(4.392) Hz and hM4D 2.833(1.408) Hz; median
538 instantaneous frequency: mCherry control 11.173(7.187) Hz and hM4D 4.204(1.997) Hz; amplitude:
539 mCherry control 21.764(9.897) pA and hM4D 24.043(13.508) pA. All reported values are
540 Median(Interquartile Range). **f**, Graph of the cumulative firing distribution for sEPSCs in L V/VI
541 thalamic-projecting pyramidal cells in the mPFC, IEI represents the interevent-interval between
542 spontaneous events. **g**, sIPSC frequency (right) and median instantaneous frequency (middle) is
543 significantly reduced in thalamic-projecting cortical cells following adolescent thalamic inhibition
544 relative to control mice, but sIPSC amplitude (left) is unchanged; mCherry control, $n = 19$ cells and
545 4 animals; hM4D, $n = 26$ cells and 5 animals; frequency: mCherry control 4.917(1.825) Hz and
546 hM4D 2.100(1.350) Hz; median instantaneous frequency: mCherry control 7.896(4.100) Hz and
547 hM4D 2.755(2.081) Hz; amplitude: mCherry control 19.267(7.264) pA and hM4D 15.720(7.127) pA.
548 All reported values are Median(Interquartile Range). **h**, Graph of the cumulative firing distribution
549 for sIPSCs in L V/VI thalamic-projecting pyramidal cells in the mPFC. *P<0.05.
550

551 **Figure 4) Adolescent thalamocortical activity results in enhanced amplitude in deeper (V/VI)**
552 **accumbens-projecting cortical cells. a**, Adolescent experimental timeline and schematic. Whole-
553 cell patch clamp recordings were made from accumbens-projecting pyramidal cells in layer V/VI of
554 the mPFC from hM4D and control mice; Created with https://biorender.com. **b**, Example image
555 illustrating rgGFP positive, accumbens-projecting cells in the prelimbic subregion of the medial
556 prefrontal cortex, Layer V/VI (yellow outline). Scale bar represents 500µm. **c**, Representative traces
557 showing sEPSCs of hM4D animals and mCherry controls. **d**, Representative traces showing sIPSCs
558 of hM4D animals and mCherry controls**. e**, sEPSC amplitude (left) is significantly increased in
559 accumbens-projecting cortical cells following adolescent thalamic inhibition relative to control mice,
560 but sEPSC frequency (right) and median instantaneous frequency (middle) are unchanged; mCherry
561 control, $n = 22$ cells and 5 animals; hM4D, $n = 9$ cells and 4 animals; frequency: mCherry control
562 4.450(2.012) Hz, hM4D 3.167(4.217) Hz.; median instantaneous frequency: mCherry control
563 7.371(4.043) Hz and hM4D 5.290(12.190) Hz; amplitude: mCherry control 20.460(11.638) pA and
564 hM4D 29.858(5.869). All reported values are Median(Interquartile Range). **f**, Graph of the
565 cumulative firing distribution for sEPSCs in L II/III accumbens-projecting pyramidal cells in the
566 mPFC, IEI represents the interevent-interval between spontaneous events. **g**, sIPSC frequency (right)
567 is significantly reduced in accumbens-projecting cortical cells following adolescent thalamic
568 inhibition relative to control mice, but sIPSC amplitude (left) and median instantaneous frequency
569 (middle) are unchanged; mCherry control, $n = 21$ cells and 5 animals; hM4D, $n = 28$ cells and 6
570 animals; frequency: mCherry control 1.883(1.817) Hz, hM4D 2.50(2.350) Hz; median instantaneous
571 frequency: mCherry control 2.997(2.405) Hz and hM4D 4.005(4.349) Hz; amplitude: mCherry
572 control 13.362(2.306) pA and hM4D 17.495(3.331). All reported values are Median(Interquartile

573 Range). **h**, Graph of the cumulative firing distribution for sIPSCs in L V/VI accumbens-projecting
574 pyramidal cells in the mPFC. *P<0.05.
575
576
577 **Figure 5) Adolescent thalamocortical activity regulates cross-hemispheric inhibition. a**,
578 Adolescent experimental timeline and schematic. Whole-cell patch clamp recordings were made
579 from cortical-projecting pyramidal cells in layer II/III of the mPFC from hM4D and control mice;
580 Created with https://biorender.com. **b**, Example image illustrating rgGFP positive, cortical-
581 projecting cells in the prelimbic subregion of the medial prefrontal cortex (orange outline). Virus was
582 injected into the dextral (right) hemisphere and cells were recorded only in the sinistral (left)
583 hemisphere. Scale bar represents 500µm. **c**, Representative traces showing sEPSCs of hM4D animals
584 and mCherry controls. **d**, Representative traces showing sIPSCs of hM4D animals and mCherry
585 controls**. e**, sEPSC frequency (right), sEPSC amplitude (left) and sEPSC median instantaneous
586 frequency are unchanged in cortical-projecting cortical cells following adolescent thalamic inhibition
587 relative to control mice; mCherry control, $n = 38$ cells and 5 animals; hM4D, $n = 26$ cells and 5
588 animals; frequency: mCherry control 3.042(1.713) Hz and hM4D 2.95(2.933) Hz; median
589 instantaneous frequency: mCherry control 4.807(3.944) Hz and hM4D 5.042(5.890) Hz; amplitude:
590 mCherry control 17.876(7.549) pA and hM4D 23.951(8.397) pA. All reported values are
591 Median(Interquartile Range). **f**, Graph of the cumulative firing distribution for sEPSCs in cortical-
592 projecting pyramidal cells in the mPFC, IEI represents the interevent-interval between spontaneous
593 events. **g**, sIPSC median instantaneous frequency (middle) is significantly increased and frequency
594 (right) is trending towards an increase in cortical-projecting cortical cells following adolescent
595 thalamic inhibition relative to control mice, while amplitude (left) is unchanged; mCherry
596 control, $n = 38$ cells and 5 animals; hM4D, $n = 26$ cells and 5 animals; frequency: mCherry control

597 1.233(0.954) Hz and hM4D 2.208(1.887) Hz; median instantaneous frequency: mCherry control
598 1.937(1.676) Hz and hM4D 5.551(2.498); amplitude: mCherry control 15.735(5.268) pA and hM4D
599 15.099(5.667) pA. All reported values are Median(Interquartile Range). **h**, Graph of the cumulative
600 firing distribution for sIPSCs in cortical-projecting pyramidal cells in the mPFC. *P<0.05, #P<0.10.
601
602
603 **Figure 6) Adolescent thalamocortical inhibition disrupts E/I Ratio in cortical-**
604 **projecting cortical cells. a,** Excitatory/Inhibitory ratio in nonspecific layer II/III cells for amplitude
605 (left), median instantaneous frequency (middle), and frequency (right). There was no significant difference
606 in E/I ratio between mCherry 1.188(0.400) pA/pA, hM4D 1.432(0.704) pA/pA or hM4D+Saline
607 2.005(1.247) pA/pA for amplitude [$f = 2.567$, d.f. = 2, 11.07 $P = 0.121$]. There was no significant
608 difference in E/I ratio between mCherry 2.131(2.020) Hz/Hz, hM4D 1.736(2.409) Hz/Hz or hM4D+Saline
609 2.183(1.306) Hz/Hz for median instantaneous frequency [$f = 0.713$, d.f. = 2, 11.65 $P = 0.511$]. There was
610 no significant difference in E/I ratio between mCherry 2.265(4.677) Hz/Hz, hM4D 2.186(3.134) Hz/Hz or
611 hM4D+Saline 2.490(1.325) Hz/Hz for median instantaneous frequency [$f = 1.209$, d.f. = 2, 43 $P = 0.308$].
612 **b,** Excitatory/Inhibitory ratio in layer II/III accumbens-projecting cortical cells for amplitude (left),
613 median instantaneous frequency (middle), and frequency (right). There was no significant difference in
614 E/I ratio between mCherry 1.316(0.587) pA/pA or hM4D 1.524(0.505) pA/pA for amplitude [$f = 0.543$,
615 d.f. = 1, 6.59 $P = 0.487$]. There was no significant difference in E/I ratio between mCherry
616 1.686(1.368) Hz/Hz and hM4D 1.999(1.715) Hz/Hz for median instantaneous frequency [$f = 0.836$,
617 d.f. = 1, 7.91 $P = 0.388$]. There was no significant difference in E/I ratio between mCherry
618 1.663(0.963) Hz/Hz and hM4D 1.865(1.406) Hz/Hz for frequency [$f = 0.750$, d.f. = 1, 8.10 $P = 0.411$]. **c,**
619 Excitatory/Inhibitory ratio in layer V/VI thalamic-projecting cortical cells for amplitude (left), median

instantaneous frequency (middle), and frequency (right). There was no significant difference in E/I ratio between mCherry 1.195(0.500) pA/pA or hM4D 1.376(0.858) pA/pA for amplitude [$f = 3.625$, d.f. = 1, 42 $P = 0.064$]. There was no significant difference in E/I ratio between mCherry 1.414(0.485) Hz/Hz and hM4D 1.660(1.143) Hz/Hz for median instantaneous frequency [$f = 0.975$, d.f. = 1, 5.21 $P = 0.367$]. There was no significant difference in E/I ratio between mCherry 1.414(0.485) Hz/Hz and hM4D 1.503(1.136) Hz/Hz for frequency [$f = 1.115$, d.f. = 1, 5.31 $P = 0.337$]. **d,** Excitatory/Inhibitory ratio in layer V/VI accumbens-projecting cortical cells for amplitude (left), median instantaneous frequency (middle), and frequency (right). There was no significant difference in E/I ratio between mCherry 1.467(0.624) pA/pA or hM4D 1.730(0.618) pA/pA for amplitude [$f = 2.220$, d.f. = 1, 28 $P = 0.147$]. There was no significant difference in E/I ratio between mCherry 2.060(1.840) Hz/Hz and hM4D 2.432(1.435) Hz/Hz for median instantaneous frequency [$f = 0.412$, d.f. = 1, 12.33 $P = 0.533$]. There was no significant difference in E/I ratio between mCherry 1.829(1.623) Hz/Hz and hM4D 2.658(1.765) Hz/Hz for frequency [$f = 0.014$, d.f. = 1, 12.10 $P = 0.908$]. **e,** Excitatory/Inhibitory ratio in cortical-projecting cortical cells for amplitude (left), median instantaneous frequency (middle), and frequency (right). There was no significant difference in E/I ratio between mCherry 1.209(0.359) pA/pA or hM4D 1.473(0.403) pA/pA for amplitude [$f = 1.099$, d.f. = 1, 59 $P = 0.299$]. There was a significant decrease in E/I ratio between mCherry 2.513(1.915) Hz/Hz and hM4D 1.517(1.670) Hz/Hz for median instantaneous frequency. There was also a significant decrease in E/I ratio between mCherry 2.594(1.607) Hz/Hz and hM4D 1.564(1.544) Hz/Hz for frequency. All reported values are Median(Interquartile Range). *P<0.05.

Figure 7) P20-P35 thalamocortical inhibition produces cognitive deficits in adult mice. a, Adolescent experimental timeline, and schematic. J60 was administered from P20-P35 to mice expressing hM4D or a control fluorophore (GFP) in the thalamus. Behavioral testing was conducted 55 days later, at P90. Created with https://biorender.com **b,** Representative image of hM4D expression in the MD of adult mice. Scale bar represents 300µm. **c,** Representative viral spread of hM4D receptor in mice that underwent the ASST task. **d,** Schematic of the attentional set-shifting task (ASST). Mice were trained to associate a cinnamon scent with a reward irrespective of bedding medium (IA). After meeting criterion, an extra-dimensional set shift occurred (EDSS) and mice had to associate the paper bedding with a reward irrespective of scent. Red is representative of the rewarded stimulus. **e,** Adolescent-inhibited hM4D animals are no different than controls in the initial acquisition (IA) of the ASST (left, Control: n=11 animals, 14.27± 2.276 trials, hM4D: n=13 animals, hM4D: 12.08±2.276 trials; two-sided unpaired t-test, t=0.9647, df=22, p=0.3452) but take significantly more trials in the extra-dimensional set shift (EDSS) than controls (right, Control: n=11 animals, 10.73±1.871 trials, hM4D: n=13 animals, hM4D: 14.92±1.871 trials; unpaired t-test, t=2.442, df=22, *p=0.0354). **f,** Adolescent-inhibited hM4D animals committed more perseverative errors (P. Err.) than control animals (left, Control: n=11 animals, 1.091±0.7759 trials, hM4D: n=13 animals, hM4D: 3.000±0.7759 trials; unpaired t-test, t=2.461, df=22, *p=0.0222). Perseverative errors are when the mouse continues with the same response strategy following a rule switch. Adolescent-inhibited hM4D animals committed more random errors (P. Err.) than control animals (right, Control: n=11 animals, 1.182±0.9010 trials, hM4D: n=13 animals, hM4D: 3.692±0.9010 trials; unpaired t-test, t=2.786, df=22, *p=0.0108) non-perseverative errors are generally considered to be random.

References:

Ahrlund-Richter S, Xuan Y, van Lunteren JA, Kim H, Ortiz C, Pollak Dorocic I, Meletis K, Carlen M (2019) A whole-brain atlas of monosynaptic input targeting four different cell types in the medial prefrontal cortex of the mouse. Nature neuroscience 22:657-668.

Anastasiades PG, Carter AG (2021) Circuit organization of the rodent medial prefrontal cortex. Trends in neurosciences 44:550-563.

Anastasiades PG, Marlin JJ, Carter AG (2018) Cell-Type Specificity of Callosally Evoked Excitation and Feedforward Inhibition in the Prefrontal Cortex. Cell reports 22:679-692.

Benoit LJ, Holt ES, Posani L, Fusi S, Harris AZ, Canetta S, Kellendonk C (2022) Adolescent thalamic inhibition leads to long-lasting impairments in prefrontal cortex function. Nature neuroscience 25:714-725.

Bhattacherjee A, Djekidel MN, Chen R, Chen W, Tuesta LM, Zhang Y (2019) Cell type-specific transcriptional programs in mouse prefrontal cortex during adolescence and addiction. Nature communications 10:4169.

Bonaventura J et al. (2019) High-potency ligands for DREADD imaging and activation in rodents and monkeys. Nature communications 10:4627.

Canetta S, Teboul E, Holt E, Bolkan SS, Padilla-Coreano N, Gordon JA, Harrison NL, Kellendonk C (2020) Differential Synaptic Dynamics and Circuit Connectivity of Hippocampal and Thalamic Inputs to the Prefrontal Cortex. Cereb Cortex Commun 1:tgaa084.

Chini M, Hanganu-Opatz IL (2021) Prefrontal Cortex Development in Health and Disease: Lessons from Rodents and Humans. Trends in neurosciences 44:227-240.

Cho KKA, Shi J, Phensy AJ, Turner ML, Sohal VS (2023) Long-range inhibition synchronizes and updates prefrontal task activity. Nature 617:548-554.

Collins DP, Anastasiades PG, Marlin JJ, Carter AG (2018) Reciprocal Circuits Linking the Prefrontal Cortex with Dorsal and Ventral Thalamic Nuclei. Neuron 98:366-379 e364.

Delevich K, Tucciarone J, Huang ZJ, Li B (2015) The Mediodorsal Thalamus Drives Feedforward Inhibition in the Anterior Cingulate Cortex via Parvalbumin Interneurons. The Journal of neuroscience : the official journal of the Society for Neuroscience 35:5743-5753.

Dienel SJ, Schoonover KE, Lewis DA (2022) Cognitive Dysfunction and Prefrontal Cortical Circuit Alterations in Schizophrenia: Developmental Trajectories. Biological psychiatry 92:450-459.

Feinberg I (1982) Schizophrenia: caused by a fault in programmed synaptic elimination during adolescence? Journal of psychiatric research 17:319-334.

Fuster JM (2001) The prefrontal cortex--an update: time is of the essence. Neuron 30:319-333.

Gogtay N, Vyas NS, Testa R, Wood SJ, Pantelis C (2011) Age of onset of schizophrenia: perspectives from structural neuroimaging studies. Schizophrenia bulletin 37:504-513.

Greenhill SD, Ranson A, Fox K (2015) Hebbian and Homeostatic Plasticity Mechanisms in Regular Spiking and Intrinsic Bursting Cells of Cortical Layer 5. Neuron 88:539-552.

Hasegawa I, Fukushima T, Ihara T, Miyashita Y (1998) Callosal window between prefrontal cortices: cognitive interaction to retrieve long-term memory. Science 281:814-818.

Holler-Wallscheid MS, Thier P, Pomper JK, Lindner A (2017) Bilateral recruitment of prefrontal cortex in working memory is associated with task demand but not with age. Proceedings of the National Academy of Sciences of the United States of America 114:E830-E839.

Hoops D, Flores C (2017) Making Dopamine Connections in Adolescence. Trends in neurosciences 40:709-719.

708 Kalivas PW, Volkow N, Seamans J (2005) Unmanageable motivation in addiction: a pathology in
709 prefrontal-accumbens glutamate transmission. Neuron 45:647-650.
710 Larsen B, Luna B (2018) Adolescence as a neurobiological critical period for the development of higher-
711 order cognition. Neuroscience & Biobehavioral Reviews 94:179-195.
712 Mannella F, Gurney K, Baldassarre G (2013) The nucleus accumbens as a nexus between values and
713 goals in goal-directed behavior: a review and a new hypothesis. Frontiers in behavioral
714 neuroscience 7:135.
715 Manvich DF, Webster KA, Foster SL, Farrell MS, Ritchie JC, Porter JH, Weinshenker D (2018) The
716 DREADD agonist clozapine N-oxide (CNO) is reverse-metabolized to clozapine and produces
717 clozapine-like interoceptive stimulus effects in rats and mice. Scientific reports 8:3840.
718 McGlinchey EM, James MH, Mahler SV, Pantazis C, Aston-Jones G (2016) Prelimbic to Accumbens
719 Core Pathway Is Recruited in a Dopamine-Dependent Manner to Drive Cued Reinstatement of
720 Cocaine Seeking. The Journal of neuroscience : the official journal of the Society for
721 Neuroscience 36:8700-8711.
722 Miller EK, Lundqvist M, Bastos AM (2018) Working Memory 2.0. Neuron 100:463-475.
723 Nabel EM, Morishita H (2013) Regulating critical period plasticity: insight from the visual system to
724 fear circuitry for therapeutic interventions. Front Psychiatry 4:146.
725 Nabel EM, Garkun Y, Koike H, Sadahiro M, Liang A, Norman KJ, Taccheri G, Demars MP, Im S, Caro
726 K, Lopez S, Bateh J, Hof PR, Clem RL, Morishita H (2020) Adolescent frontal top-down
727 neurons receive heightened local drive to establish adult attentional behavior in mice. Nature
728 communications 11:3983.
729 Okun M, Lampl I (2008) Instantaneous correlation of excitation and inhibition during ongoing and
730 sensory-evoked activities. Nature neuroscience 11:535-537.
731 Paus T, Keshavan M, Giedd JN (2008) Why do many psychiatric disorders emerge during adolescence?
732 Nature reviews Neuroscience 9:947-957.
733 Pi HJ, Hangya B, Kvitsiani D, Sanders JI, Huang ZJ, Kepecs A (2013) Cortical interneurons that
734 specialize in disinhibitory control. Nature 503:521-524.
735 Sakurai T, Gamo NJ (2019) Cognitive functions associated with developing prefrontal cortex during
736 adolescence and developmental neuropsychiatric disorders. Neurobiology of Disease
737 131:104322.
738 Sun Q, Li X, Ren M, Zhao M, Zhong Q, Ren Y, Luo P, Ni H, Zhang X, Zhang C, Yuan J, Li A, Luo M,
739 Gong H, Luo Q (2019) A whole-brain map of long-range inputs to GABAergic interneurons in
740 the mouse medial prefrontal cortex. Nature neuroscience 22:1357-1370.
741 Wen W, Turrigiano GG (2021) Developmental Regulation of Homeostatic Plasticity in Mouse Primary
742 Visual Cortex. The Journal of neuroscience : the official journal of the Society for Neuroscience
743 41:9891-9905.
744 Wiesel TN, Hubel DH (1963) Single-Cell Responses in Striate Cortex of Kittens Deprived of Vision in
745 One Eye. Journal of neurophysiology 26:1003-1017.
746 Yang S, Tseng KY (2022) Maturation of Corticolimbic Functional Connectivity During Sensitive
747 Periods of Brain Development. Current topics in behavioral neurosciences 53:37-53.
748 Yang SS, Mack NR, Shu Y, Gao WJ (2021) Prefrontal GABAergic Interneurons Gate Long-Range
749 Afferents to Regulate Prefrontal Cortex-Associated Complex Behaviors. Frontiers in neural
750 circuits 15:716408.
751

Figure 1

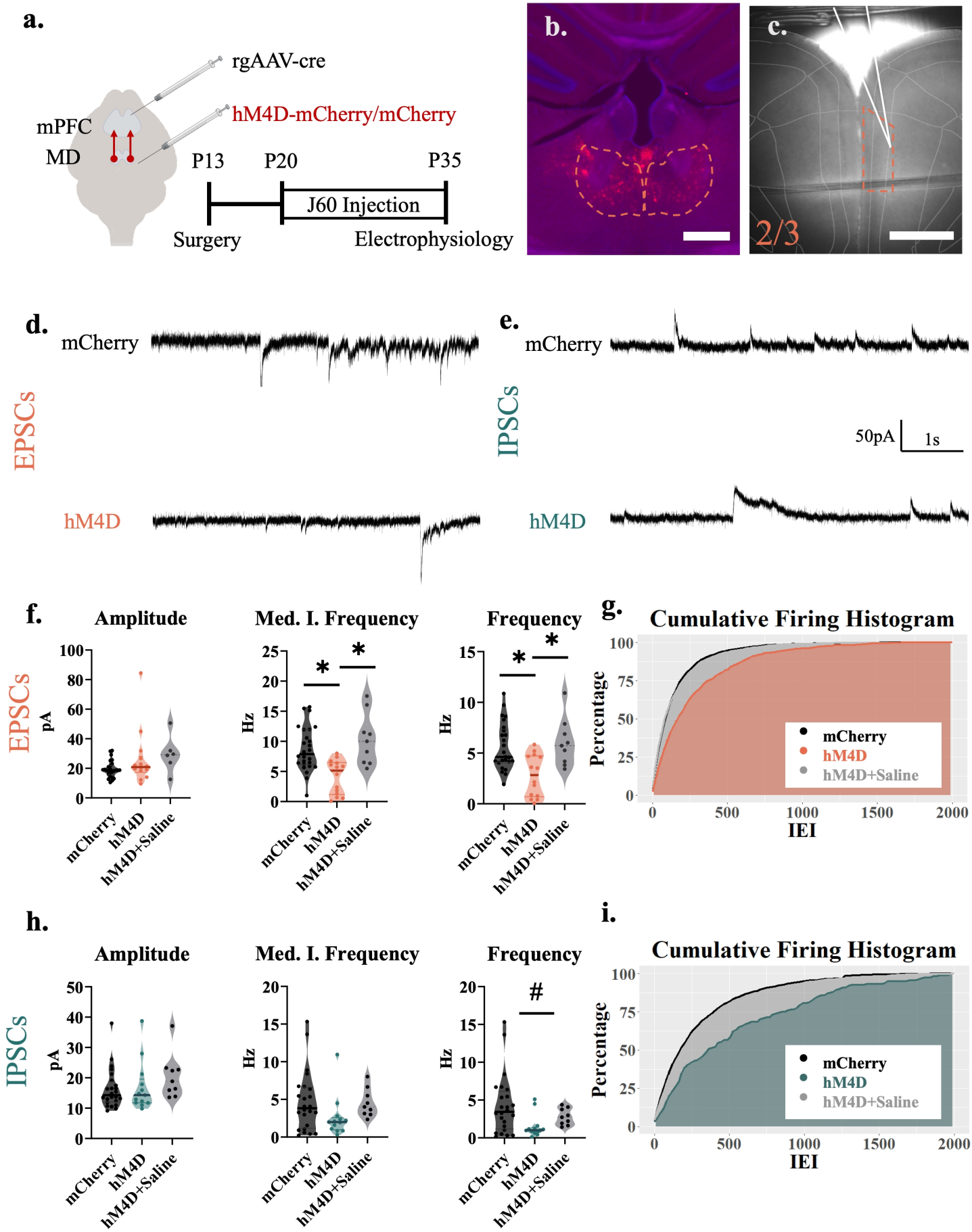
a.
rgAAV-cre
hM4D-mCherry/mCherry
mPFC
MD
P13
P20
P35
J60 Injection
Surgery
Electrophysiology
b.
c.
2/3
d.
mCherry
EPSCs
hM4D
e.
mCherry
IPSCs
50pA
1s
hM4D
f.
Amplitude
Med. I. Frequency
Frequency
EPSCs
pA
Hz
mCherry
hM4D
hM4D+Saline
g.
Cumulative Firing Histogram
Percentage
IEI
mCherry
hM4D
hM4D+Saline
h.
Amplitude
Med. I. Frequency
Frequency
IPSCs
pA
Hz
mCherry
hM4D
hM4D+Saline
i.
Cumulative Firing Histogram
Percentage
IEI
mCherry
hM4D
hM4D+Saline

Figure 2

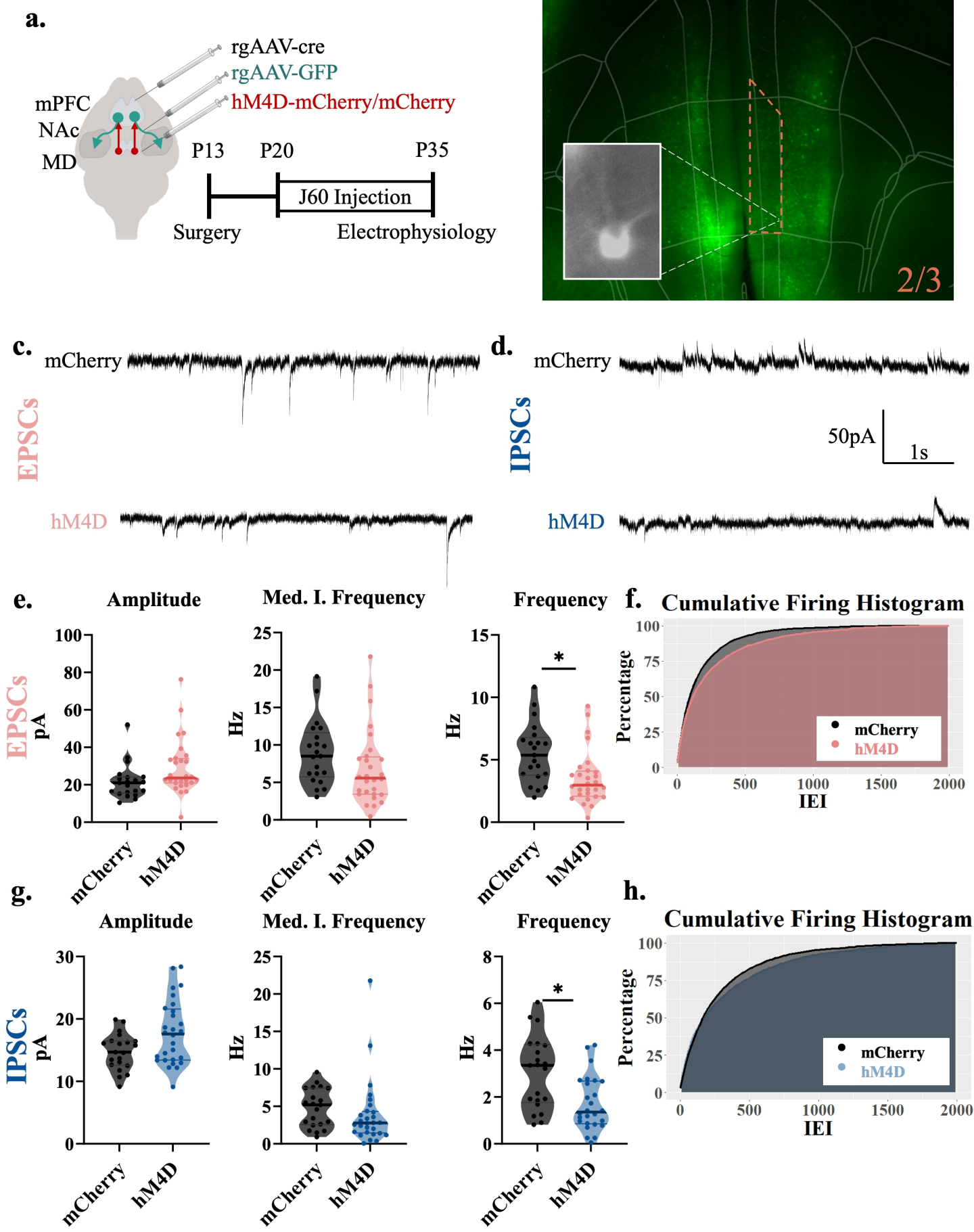
a.
rgAAV-cre
rgAAV-GFP
hM4D-mCherry/mCherry
mPFC
NAc
MD
P13
P20
P35
J60 Injection
Surgery
Electrophysiology
b.
2/3
c.
mCherry
EPSCs
hM4D
d.
mCherry
IPSCs
50pA
1s
hM4D
e.
Amplitude
Med. I. Frequency
Frequency
EPSCs
pA
Hz
Hz
mCherry
hM4D
f.
Cumulative Firing Histogram
Percentage
IEI
mCherry
hM4D
g.
Amplitude
Med. I. Frequency
Frequency
IPSCs
pA
Hz
Hz
mCherry
hM4D
h.
Cumulative Firing Histogram
Percentage
IEI
mCherry
hM4D

Figure 3

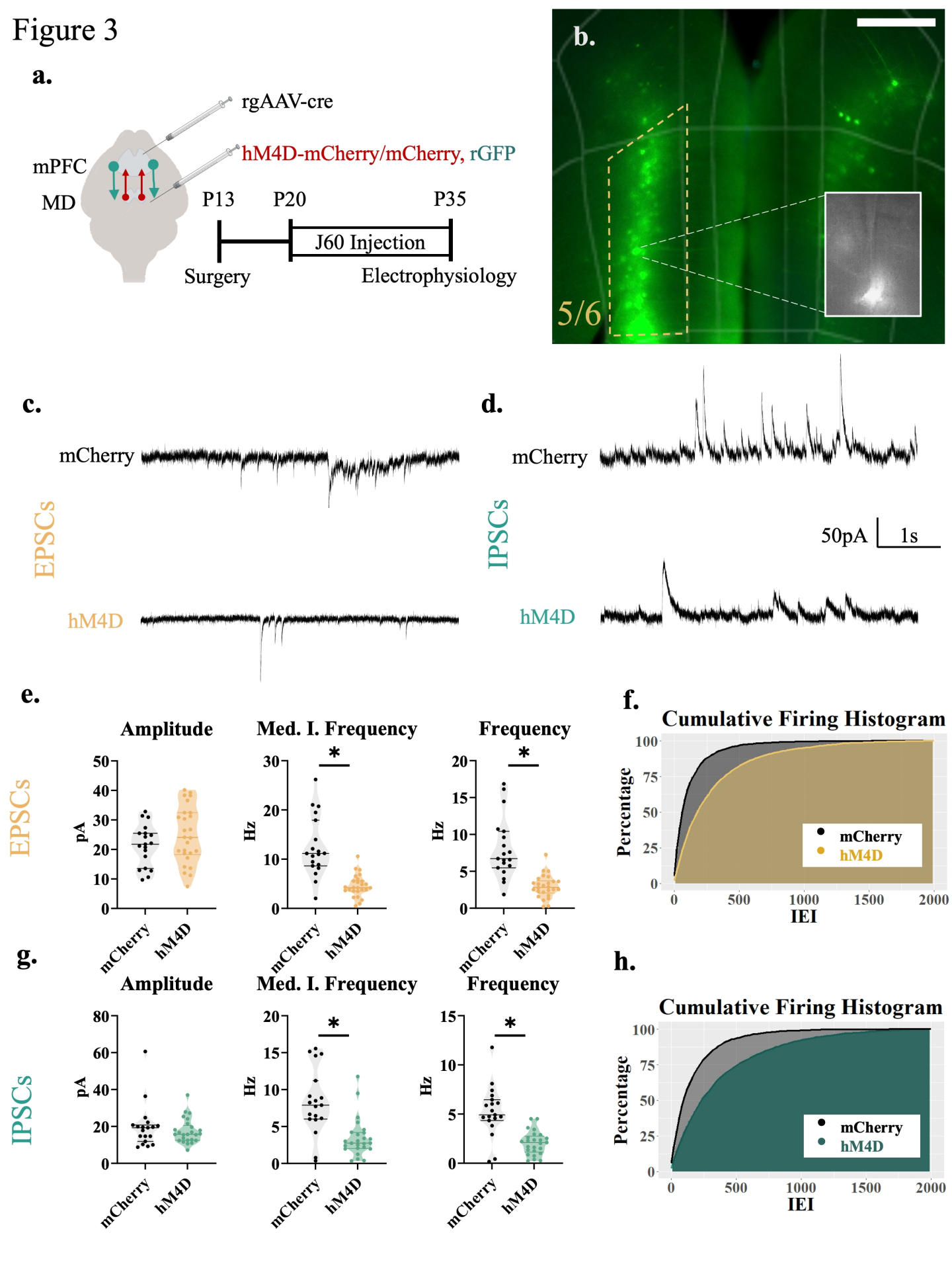
a.
rgAAV-cre
hM4D-mCherry/mCherry, rGFP
mPFC
MD
P13
P20
P35
J60 Injection
Surgery
Electrophysiology
b.
5/6
c.
mCherry
EPSCs
hM4D
d.
mCherry
IPSCs
50pA
1s
hM4D
e.
Amplitude
Med. I. Frequency
Frequency
EPSCs
pA
Hz
Hz
mCherry
hM4D
f.
Cumulative Firing Histogram
Percentage
IEI
mCherry
hM4D
g.
Amplitude
Med. I. Frequency
Frequency
IPSCs
pA
Hz
Hz
mCherry
hM4D
h.
Cumulative Firing Histogram
Percentage
IEI
mCherry
hM4D

Figure 4

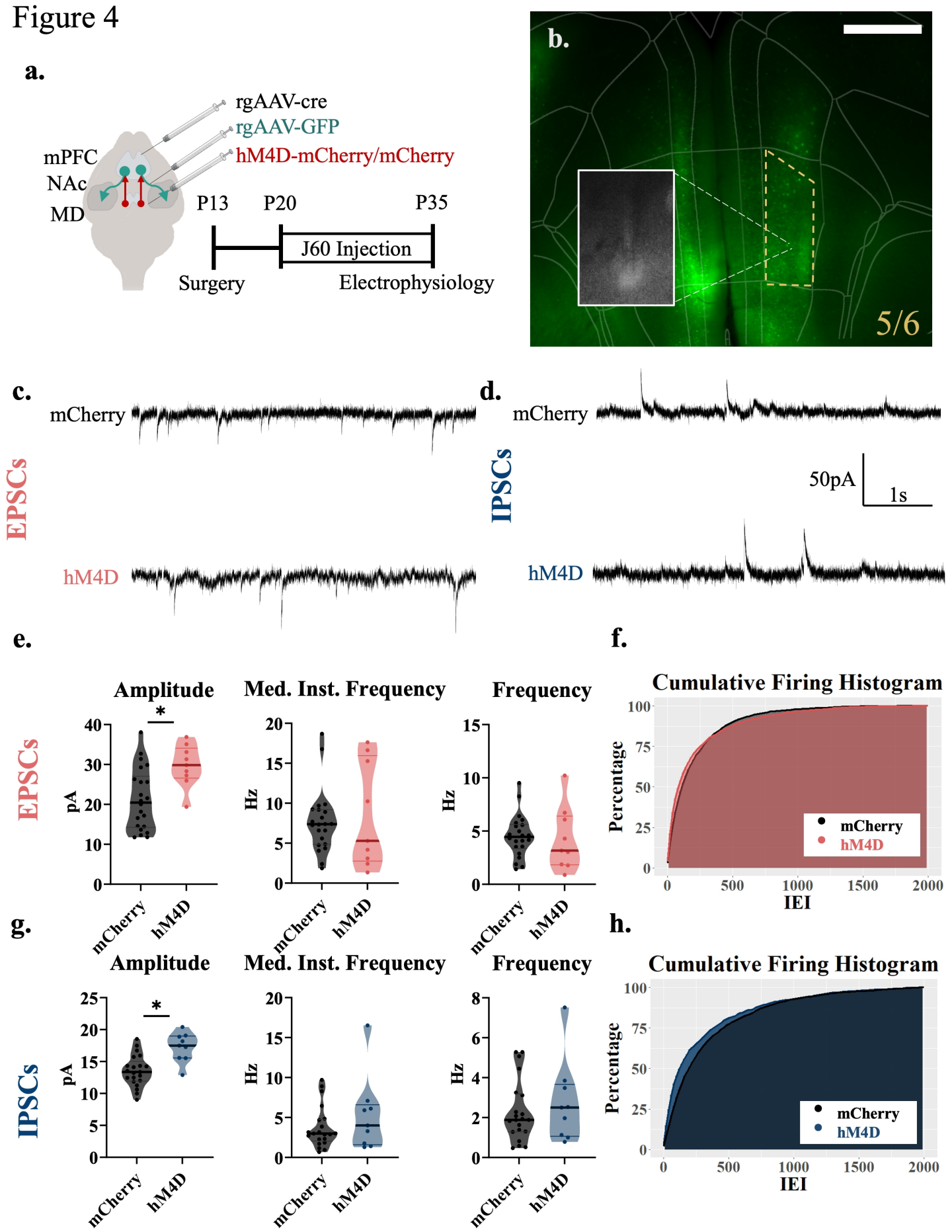
a.
rgAAV-cre
rgAAV-GFP
hM4D-mCherry/mCherry
mPFC
NAc
MD
P13
P20
P35
J60 Injection
Surgery
Electrophysiology
b.
5/6
c.
mCherry
EPSCs
hM4D
d.
mCherry
IPSCs
50pA
1s
hM4D
e.
Amplitude
Med. Inst. Frequency
Frequency
EPSCs
pA
Hz
mCherry
hM4D
f.
Cumulative Firing Histogram
Percentage
IEI
mCherry
hM4D
g.
Amplitude
Med. Inst. Frequency
Frequency
IPSCs
pA
Hz
mCherry
hM4D
h.
Cumulative Firing Histogram
Percentage
IEI
mCherry
hM4D

Figure 5

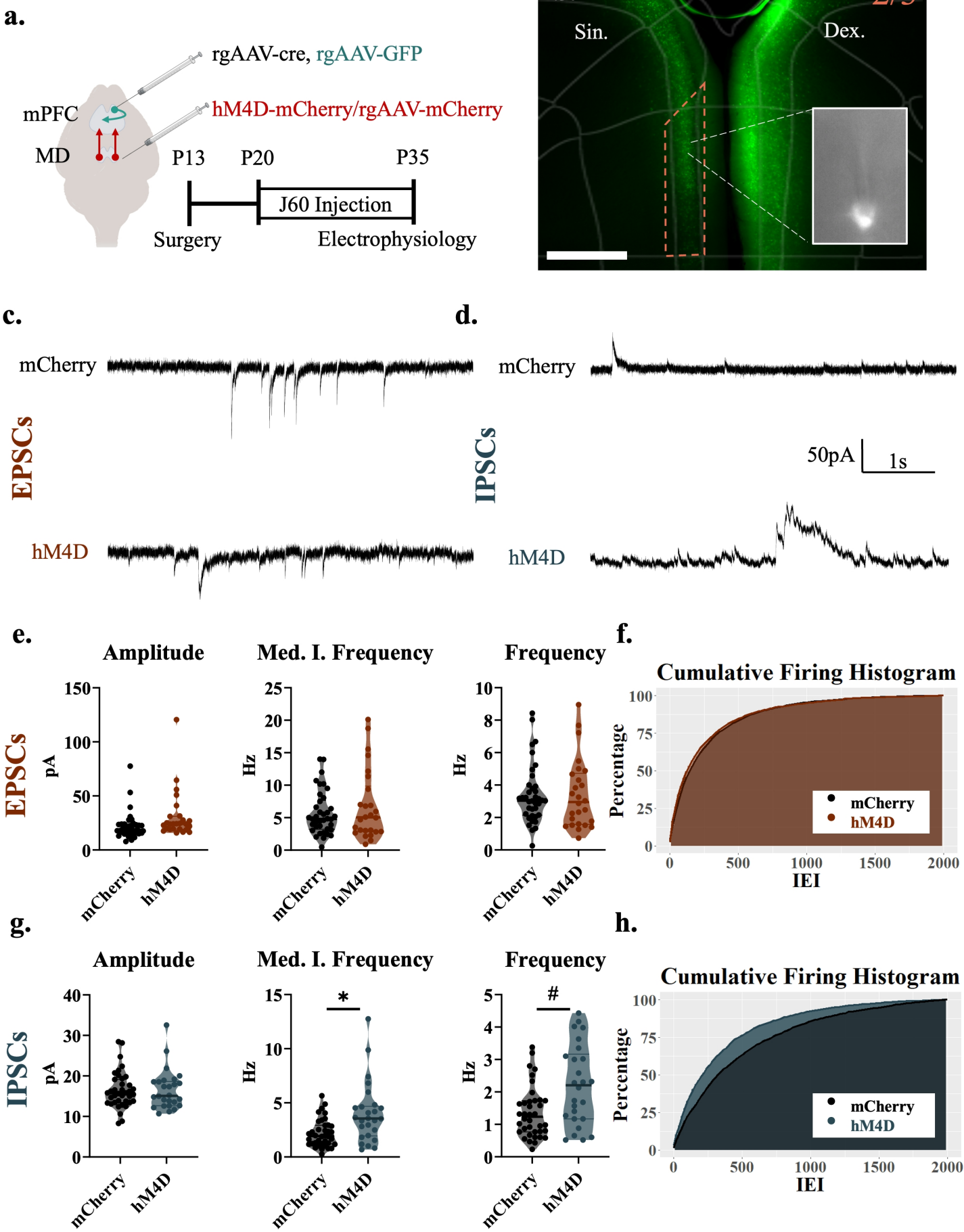
a.
rgAAV-cre, rgAAV-GFP
hM4D-mCherry/rgAAV-mCherry
mPFC
MD
P13
P20
P35
J60 Injection
Surgery
Electrophysiology
b.
2/3
Sin.
Dex.
c.
mCherry
EPSCs
hM4D
d.
mCherry
IPSCs
50pA
1s
hM4D
e.
Amplitude
Med. I. Frequency
Frequency
EPSCs
pA
Hz
Hz
mCherry
hM4D
f.
Cumulative Firing Histogram
Percentage
IEI
mCherry
hM4D
g.
Amplitude
Med. I. Frequency
Frequency
IPSCs
pA
Hz
Hz
*
#
mCherry
hM4D
h.
Cumulative Firing Histogram
Percentage
IEI
mCherry
hM4D

Figure 6

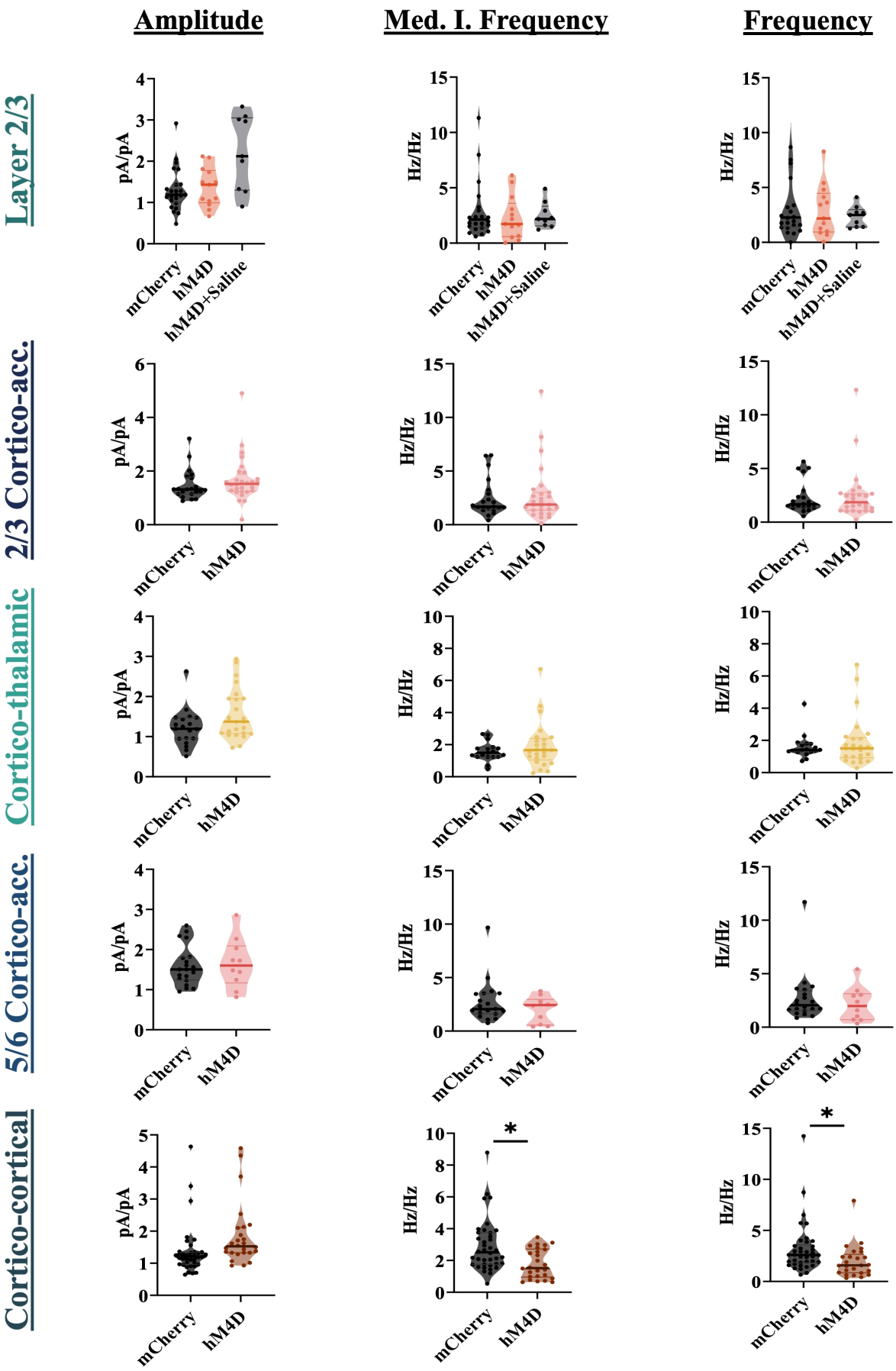
a.
Amplitude
Med. I. Frequency
Frequency
Layer 2/3
pA/pA
Hz/Hz
mCherry
hM4D
hM4D+Saline
b.
2/3 Cortico-acc.
c.
Cortico-thalamic
d.
5/6 Cortico-acc.
e.
Cortico-cortical
*

Figure 7

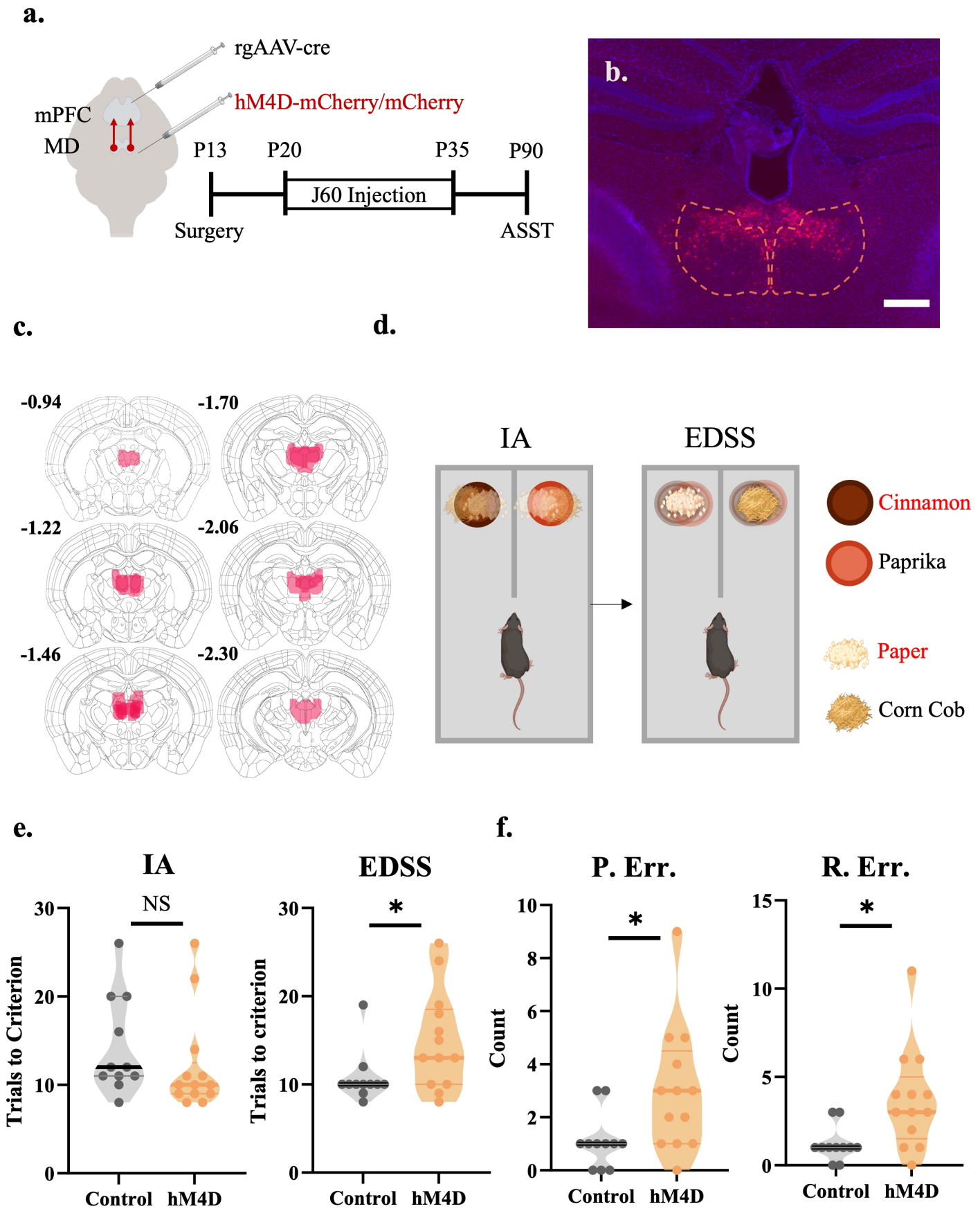
a.
rgAAV-cre
hM4D-mCherry/mCherry
mPFC
MD
P13
P20
P35
P90
J60 Injection
Surgery
ASST
b.
c.
-0.94
-1.70
-1.22
-2.06
-1.46
-2.30
d.
IA
EDSS
Cinnamon
Paprika
Paper
Corn Cob
e.
IA
EDSS
NS
*
Trials to Criterion
Trials to criterion
Control
hM4D
f.
P. Err.
R. Err.
*
*
Count
Control
hM4D